Sanchis-Perucho, P.; Robles Martínez, Á.; Durán, F.; Ferrer, J.; Seco, A. (2020). PDMS membranes for feasible recovery of dissolved methane from AnMBR effluents. Journal of Membrane Science. 604:1-12. https://doi.org/10.1016/j.memsci.2020.118070

PDMS membranes for feasible recovery of dissolved methane from AnMBR effluents

Pau Sanchis-Perucho [a*], Ángel Robles [a], Freddy Durán [b], José Ferrer [c], Aurora Seco [a]

[a] CALAGUA – Unidad Mixta UV-UPV, Departament d'Enginyeria Química, Universitat de València, Spain. (e-mail: pau.sanchis-perucho@uv.es; angel.robles@uv.es; aurora.seco@uv.es)

[b] FCC Aqualia, S.A., Spain. (e-mail: freddy.duran@fcc.es)

[c] CALAGUA – Unidad Mixta UV-UPV, Institut Universitari d'Investigació d'Enginyeria de l'Aigua i Medi Ambient – IIAMA, Universitat Politècnica de Valencia, Spain. (e-mail: jferrer@hma.upv.es)

*Corresponding author: pau.sanchis-perucho@uv.es

ABSTRACT

This study aimed to evaluate the feasibility of degassing membrane (DM) technology for recovering dissolved methane from AnMBR effluents. For that purpose, a PDMS membrane module was operated for treating the effluent from an AnMBR prototype-plant, which treated urban wastewater (UWW) at ambient temperature. Different transmembrane pressures and liquid flow rates were applied for evaluating methane recovery efficiency. Maximum methane recoveries were achieved when increasing the vacuum pressure and reducing the liquid flow rate, reaching a maximum methane recovery efficiency of around 80% at a transmembrane pressure (TMP) of 0.8 bars and a treatment flow rate (Q_L) of 50 L h^{-1}. The results revealed that the combination of PDMS DMs and AnMBR technology would allow to reduce the energy demand of UWW treatment, achieving net energy productions while reducing greenhouse gas emissions. Optimum operation was determined at a TMP of 0.8 bars and a Q_L of 150 L h^{-1} when combining energy, environmental and economic targets. Under these operating conditions, the combination AnMBR+DM resulted in energy requirements and greenhouse gases emissions of -0.040 kWh and 0.113 kg of CO_2-eq per m^3 of treated water, respectively, resulting in a DM payback period of around 10.5 years.

Keywords

Anaerobic membrane bioreactor (AnMBR); greenhouse gas (GHG); methane recovery; PDMS degassing membrane; urban wastewater.

1. INTRODUCTION

Urban wastewater (UWW) treatment is currently based on aerobic technology, which can result in high energy demands and high sludge productions compared to anaerobic processes [1,2]. Besides, this technology presents a limited potential for resource recovery from wastewater, which can be considered a carrier of energy, nutrients and reclaimed water [3,4]. Hence, different anaerobic configurations have emerged as an attractive alternative for UWW treatment as a result of several potential advantages, such as: (i) reduced sludge production due to the lower anaerobic biomass yield compared to aerobic microorganisms, (ii) reduced energy demand since no aeration is required for removal of organics, and (iii) enhanced energy balance by the biogas production from the degradation of organic carbon [5].

Anaerobic membrane bioreactor (AnMBR) technology has been reported by several authors as a potential alternative for full-scale low-strength wastewater treatment (e.g. [6-10]). By decoupling sludge and hydraulic retention times, AnMBR can perform suitable UWW treatment even operating at low/middle temperatures since the generated biomass is retained by the membrane [4,11]. However, direct greenhouse gas (GHG) emissions due to methane stripping from AnMBR effluents is still a key issue that limits the full-scale application of this technology [5]. Methane lost dissolved in the effluent can exceed the 80% of total methane production when the system is operated at low temperatures (e.g. 15 ºC) [12,13], resulting in significant decreases in process energy efficiency while increasing the carbon footprint of the system. Hence, the efficient recovery of this dissolved methane is imperative to develop more energy-efficiency and environmentally-friendly AnMBR systems.

Several technologies have been traditionally applied to remove dissolved gases from liquid streams (e.g. spray aeration towers, free fall jet towers, packed columns, tray aerators or diffused aerators, membrane contactors) [14]. Nevertheless, the direct contact between liquid and gas phases performed in degasification towers frequently entails operational problems such as flooding, foaming and emulsion [15]. Moreover, the sweep gas flux required in these systems involves a dilution of the collected methane, thereby reducing dramatically its energy conversion potential. Otherwise, biological technologies can be also applied to remove dissolved methane from anaerobic effluents. Aerobic methane oxidation (AMO) and aerobic methanotrophy are the most prevalent microbial pathways [16]. In AMO, an electron acceptor is required for methane oxidation, commonly using sulfate reduction or denitrification as associate processes. Specifically, the use of denitrification via nitrite or nitrate reduction has been extensively studied [17,18] since AMO can be also employed as a nitrogen removal process. However, anaerobic processes generally reduce all present sulfate and do not produces nitrite or nitrate via ammonia oxidation, thus AMO may require an additional step to treat these effluents. Aerobic methanotrophy has been also considered for dissolved methane removal from anaerobic effluents [19,20]. Matsuura *et al.* [20] achieved methane removal efficiencies up to 99% when operating a two-in-series down-flow hanging sponge reactor. Nevertheless, although this strategy can prevent GHG emissions, does not allow maximizing energy recovery due to dissolved methane consumption and energy input from oxygen supply [16]. Finally, microbial cell fuels (MCF) have been presented as an interesting alternative for the post-treatment of anaerobic effluents. This technology employs the metabolism of certain microorganisms to directly collect electrons in an anode during organic or inorganic matter oxidation thereby valorizing dissolved methane. In this respect, Chen *et al.* [16] showed that energy-neutral MCFs can be achieved by

84 solely dissolved methane consumption, reaching methane removal efficiencies of up to
85 85%. However, the performed methane-driven MCFs studies are generally conducted at
86 relatively high temperatures (from 30 to 37 ºC) [16,21,22]. Indeed, Chen *et al.* [23]
87 showed that voltage production abruptly decreases at operating temperatures around 10
88 ºC, which may represent a drawback when combined with an AnMBR operated at low
89 temperatures.

90 Degassing membrane (DM) technology has been extensively applied in several industries
91 for dissolved gasses removal from liquid streams [24]. The main advantages of this
92 technology reside in avoiding the direct contact between liquid and gas phases being the
93 oxygen removal from the water used in cooling towers the most notable application
94 [24,25]. Moreover, the dilution of recovered gases is prevented when the membrane is
95 operated at vacuum filtration. Hence, the use of DMs for methane capture is an interesting
96 approach for the treatment of anaerobic effluents since not only direct GHG emissions
97 can be prevented but also captured dissolved methane can be potentially employed for
98 energy production [13,24,26-30]. Microporous DMs are extensively recommended due
99 to high recovery efficiencies associated to their lower resistance to mass flux when
100 membrane pores are occupied with gas [24,31]. However, depending on DM material and
101 operating conditions, liquid may fill membrane pores, resulting in the so-called wetting
102 phenomenon which is intensified as liquid flow rate increases [27,32]. Under these
103 conditions, microporous DM permeate flux strongly decreases, dramatically reducing the
104 gasses capture efficiency. To overcome this limitation, non-porous membranes can be
105 applied for high-rate treatment since them are not susceptible to pore wetting. Among
106 non-porous membranes, different materials can be used for dissolved methane capture
107 such as polyamide, polypropylene or acetate cellulose [26]. Nevertheless, since carbon
108 dioxide is usually more selective that methane in polymeric membranes, non-meaningful

process enhancement can be obtained from selectivity. Thus, PDMS represents an interesting approach due to their higher gases permeability [26], which results in lower energy requirements for dissolved gasses capture from liquid streams.

So far, few studies have proved the energy feasibility of DMs for treating anaerobic effluents. Crone *et al.* [24] estimated that an energy-neutral DM operation could be reached by valorizing the recovered methane, while Henares *et al.* [28] showed that it is possible to reach net energy productions. Nevertheless, neither economic nor energy evaluations have been performed to determine the feasibility of coupling DM and AnMBR at full-scale. In addition, carbon footprint must also be taken into account since direct and indirect GHG emissions can be mitigated by increasing energy recovery and enhancing dissolved methane capture, respectively. Therefore, further studies evaluating the economic and environmental feasibility of DM technology for full-scale application are required.

This work aimed to assess the suitability of applying DM technology for treating the effluent from an AnMBR prototype-plant, determining the optimum operational conditions focusing on energy, economic and environmental targets.

2. MATERIALS AND METHODS

2.1. Experimental set-up

The DM used in this study consisted in a hollow-fiber commercial module of polydimethylsiloxane (PDMS) provided by PermSelect®, MedArray Inc. USA. The main proprieties of this DM are shown in Table 1.

131 **Table 1.** Main proprieties of the degassing membrane module

Membrane material	PDMS (Silicone)
Membrane type	Dense hollow fiber
Fiber inner diameter (μm)	190
Fiber outer diameter (μm)	300
Fiber wall thickness (μm)	55
Number of fibers	30,000
Total membrane area* (m^2)	2.1
Module length (cm)	14.2
Module diameter (cm)	8.9
Lumen side volume (mL)	205
Shell side volume (mL)	190

132 *Based on fiber outer diameter

133 The DM unit treated the methane-saturated effluent from an AnMBR prototype-plant
134 located in the 'Alcázar de San Juan' WWTP (Ciudad Real, Spain). The AnMBR
135 prototype-plant consisted in an anaerobic reactor with 40 m^3 of total volume connected
136 to three external membrane tanks (0.8 m^3 each) fitted with three ultrafiltration membrane
137 systems (PURON® PSH 41, Koch Membrane Systems, 0.03 μm pore size), giving a total
138 filtration area of 123 m^2. A fraction of the produced biogas is recycled to the anaerobic
139 reactor and the membrane tanks in order to favor the stripping of the produced gases from
140 the liquid phase thus avoiding methane super-saturation in water. Moreover, the biogas
141 injected into the membrane tank is also employed to scour the membranes thereby
142 minimizing cake layer formation on the membrane surface. The AnMBR prototype-plant
143 was operated at ambient temperature (18 ºC) and was fed with the effluent from the pre-
144 treatment of the full-scale WWTP. Further details about the AnMBR prototype-plant can
145 be found in [33]. Operational conditions and average effluent characteristics of the
146 AnMBR during the experimental period are shown in Table 2.

147 **Table 2.** Operational conditions and average effluent composition of the AnMBR system

Parameter	Mean ± SD
SRT (d)	70 ± 1
HRT (h)	27 ± 2
T (ºC)	18 ± 1
pH	7.0 ± 0.2
COD (mg COD L^{-1})	115 ± 15
VFA (mg COD L^{-1})	9 ± 5
Alk (mg $CaCO_3$ L^{-1})	1028 ± 198
TN (mg N L^{-1})	47 ± 4
TP (mg N L^{-1})	7 ± 3
S^{2-} (mg S L^{-1})	233 ± 66
Dissolved CH_4 (mg CH_4 L^{-1})	12.01 ± 0.18

148 The DM module was operated by shell-side mode, recovering the permeate gas in the
149 lumen side of the fibers. Previous experiences revealed clogging of the fibers when the
150 DM was operated at lumen-side (data not shown). This effect was attributed to the high
151 sulfide concentration in the treated effluent (see Table 2), which could form metal sulfides
152 or sulfur depositions in the inner of the fibers. Thus, shell-side operation was selected to
153 prevent clogging-related problems.

154 The driving force for methane capture was vacuum pressure, using a blower to set the
155 transmembrane pressure (TMP) between 0.2 and 0.8 bars. TMP was monitored and
156 controlled by two pressure sensors (UNIK 5000-746-3600, Druck) disposed at liquid and
157 gas sides. A gas-flow meter (TG0.5/5, Ritter) was employed to measure the permeate gas
158 flow rate. Moreover, the liquid flow rate was measured by a liquid-flow meter (VX100-
159 45, Vogelsang). Eight liquid flow rates were evaluated: from 50 to 400 L h^{-1}. Fig. 1 shows
160 a flow diagram of the wastewater treatment scheme.

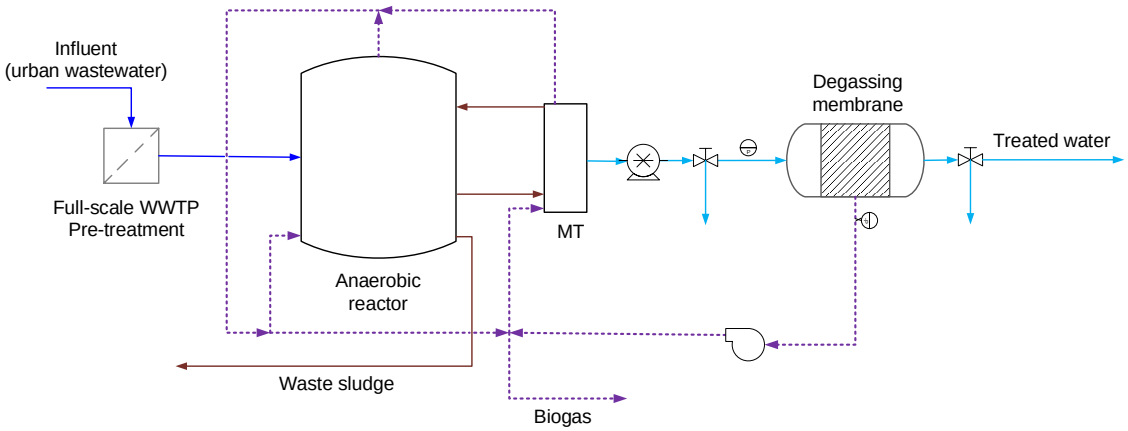

161

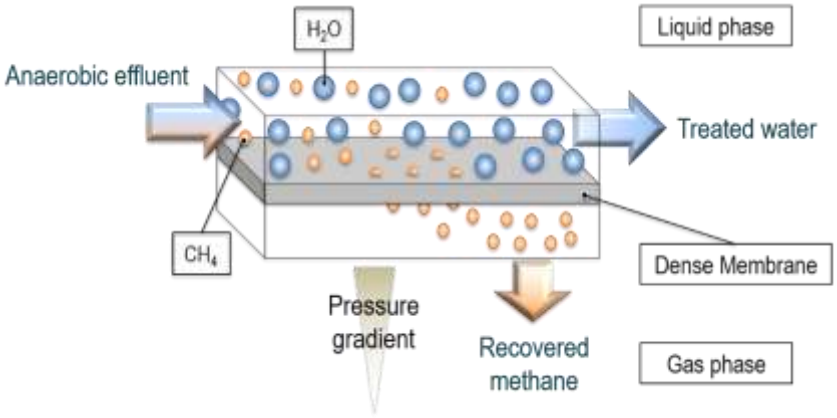

162

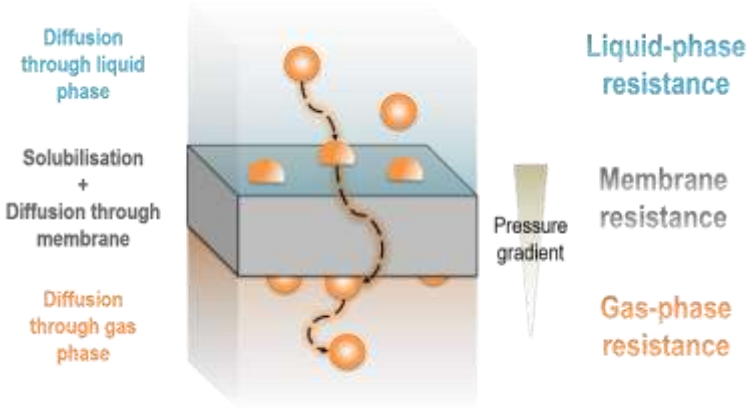

163

164 *Fig. 1. Dense DMs use for dissolved methane capture: (a) scheme of the wastewater treatment system, (b) methane*
165 *recovery mechanism, and (c) resistance-in-series model.*

166 **2.2. Analytical methods**

167 The concentration of dissolved methane from the liquid effluent was determined through
168 the head-space method described in [11]. Liquid samples were collected in 50 mL glass
169 vials from inlet and outlet of the DM to determine the recovery methane efficiency. The
170 sampling was performed in duplicate for each experimental essay. The vials collected

were stored at 20 ºC and continuous stirring was provided (at least for 4 hours) in order to achieve gas-liquid thermodynamic equilibrium. Tedlar bags of 1 L (Sigma-Aldrich) were used to collect gas samples from the recovered gas for each experimental essay.

The methane fraction reached in head-space vials and recovered gas was determined through a gas chromatograph, which was equipped with a flame ionization detector (GC-FID, Thermo Scientific). The column used was a 30 m x 0,319 mm x 25 µm HP-MOLESIEVE column (Agilent Technologies), which was operated at 40 ºC, using as carrier gas helium at a flow rate of 40 ml min^{-1}. It was injected 0.1 ml of gas samples in the gas chromatograph, using methane pure gas (99.9995%) as standard gas.

2.3. Determination of dissolved methane in the effluent

The concentration of dissolved methane from the liquid effluent ($[CH_4]_{dis}$) was calculated using the experimentally-determined head-space gas fraction (y^{CH4}) by means of the following equation:

$$[CH_4]_{dis} = \left(\frac{V_G}{V_L \cdot R \cdot T} + \frac{M^W}{H^{CH4}(T) - P \cdot y^{CH4}}\right) P \cdot \bar{M}^{CH4} \cdot y^{CH4} \quad eq.(1)$$

Where V_G and V_L are the gas and liquid volumes in collected vials (L), R is the universal constant of gases (0.082 atm L mol^{-1} K^{-1}), T is the temperature of stored vials (K), M^W is the pure water molarity (55.56 mol L^{-1}), P is the total pressure of stored vials (atm), M^{CH4} is the methane molecular weight (16 g mol^{-1}) and $H^{CH4}(T)$ is the Henrry's constant for methane. This Henrry's constant depends on temperature and can be calculated according to the following equation [34]:

$$H^{CH4}(T) = 10^{\left(\frac{-675,74}{T(K)} + 6,88\right)} \quad eq.(2)$$

The performance of the DM module was assessed by calculating the methane recovery efficiency (MRE) as follows:

$$MRE = \frac{[CH_4]_{dis.inf} - [CH_4]_{dis.eff}}{[CH_4]_{dis.inf}} \cdot 100 \quad eq.(3)$$

Where $[CH_4]_{dis.inf.}$ and $[CH_4]_{dis.eff.}$ are the concentrations of dissolved methane in influent and effluent membrane streams, respectively.

2.4. Determination of overall mass transfer coefficient

Mass transfer through membrane contactors can be evaluated by the film theory approach. Therefore, when the total resistance to mass flux (R_T) is defined as the inverse of the overall mass transfer coefficient (K_O), R_T can be interpreted as three resistances in series: the liquid phase boundary layer resistance (R_L), the permeable membrane resistance (R_M), and gas phase boundary layer resistance (R_G). The following expression can be therefore applied to describe this resistance-in-series model for cylindrical coordinates:

$$R_T = \frac{1}{K_O\, A_L} = \frac{1}{k_L\, A_L} + \frac{1}{k_m\, A_{ml}} + \frac{1}{H^{CH4}(T)\, k_G\, A_G} = R_L + R_M + R_G \quad eq.(4)$$

Where k_L, k_m and k_G are de mass transfer coefficients of liquid, membrane and gas phases, respectively, A_L and A_G are the membrane area in contact with liquid and gas phases, respectively, A_{ml} is the logarithmic mean of the membrane contactor, and $H^{CH4}(T)$ is the Henrry's constant for methane.

In liquid-gas systems, gas phase usually represents a negligible resistance for mass flux due to his higher diffusion coefficient compared to the liquid phase [35], *i.e.* $k_G >>> k_L$. Hence, *eq.* 4 can be simplified as follow:

$$\frac{1}{K_O\,A_L} = \frac{1}{k_L\,A_L} + \frac{1}{k_m\,A_{lm}} \quad eq.(5)$$

Since only liquid and membrane resistances are involved in the overall mass transfer coefficient, K_O can be calculated applying a mass balance of dissolved methane in the liquid phase, obtaining the following expression [36]:

$$Q_L \frac{\mathrm{dc}}{\mathrm{dA}} + K_O(c - c^*) = 0 \quad eq.(6)$$

Where Q_L is the liquid flow rate, A is the membrane area, c is the concentration of methane dissolved in the water and c^* is the methane concentration reached in the membrane-gas interphase, which is commonly estimated as the methane concentration in equilibrium with the gas phase (C_G):

$$c^* = H^{CH4}(T)\,c_G \quad eq.(7)$$

Therefore, employing an average value for the methane concentration reached in the gas phase (*i.e.* c^* = const.), *eq.* 6 can be integrated between the methane concentrations achieved at the inlet and outlet of the DM to obtain the following expression:

$$K_O = -\frac{Q_L}{A} \ln\left(\frac{[CH_4]_{dis.eff} - c^*}{[CH_4]_{dis.inf} - c^*}\right) \quad eq.(8)$$

Furthermore, since k_G was considered negligible and continuous vacuum was used as diving force, it could be expected that $[CH_4]_{dis} >>> c^*$, which means that $[CH_4]_{dis} - c^* \approx [CH_4]_{dis}$. Thereby, *eq.* 8 can be simplified as follows:

$$K_O = -\frac{Q_L}{A} \ln\left(\frac{[CH_4]_{dis.eff}}{[CH_4]_{dis.inf}}\right) \quad eq.(9)$$

Finally, from the combination of equations 3 and 9 the following expression linking MRE, Q_L and K_O can be deduced:

$$MRE = \left(1 - \exp\left(-\frac{A}{Q_L} K_O\right)\right) \cdot 100 \quad eq.(10)$$

2.5. Energy, GHG and economic balances

PDMS DM energy feasibility was assessed conducting an energy balance, where energy input for membrane operation and potential energy output by recovered methane were considered.

The energy production of collected gas was calculated assuming a methane power energy conversion efficiency between 30 - 40%, considering different CHP technologies applied for electricity production from biogas [37]. Although permeate pumping and gas vacuum permeation are commonly considered as energy inputs [24,28], only the power energy requirements of the blower were considered in this study. In this respect, the experiments performed in the AnMBR prototype-plant revealed that the header pressure of the AnMBR permeate (obtained by vacuum filtration) was enough to pump the liquid through the DM shell. Thus, since liquid pumping requirements are included in the energy balance of the AnMBR prototype-plant, it was not considered in the energy balance of the DM unit.

Blower power energy requirements (W) were calculated considering adiabatic compression:

$$W(J \cdot kg^{-1}) = \frac{\gamma}{\gamma - 1} \cdot \frac{R \cdot T_{IN}}{M} \left[\left(\frac{P_{OUT}}{P_{IN}}\right)^{\frac{\gamma-1}{\gamma}} - 1\right] \quad eq.(11)$$

250 Where P_{OUT} and P_{IN} are the outlet and inlet blower pressures, respectively, T_{IN} is the
251 temperature of inlet gas, M is the molecular weight of the gas and γ is the heat capacity
252 ratio. It was assumed a vacuum pump efficiency of 0.65 for the blower.

253 The environmental feasibility of PDMS DM was assessed by calculating the GHG
254 emissions related to the operation phase of the treatment scheme. Both methane capture
255 and power requirements where considered. A global warming potential (GWP) of 28 kg
256 CO_2 equivalent per kg of emitted methane [38] was considered in this study. Moreover,
257 a GWP between 0.30 – 0.40 kg CO_2 per kWh of consumed energy was considered,
258 representing the GHG emission ratio of Spain energy mix provided by different energy
259 suppliers [39].

260 For payback estimation, an energy cost between 0.05 – 0.09 € per kWh was considered
261 according to current Spain electrical rates for high voltage installations [40,41]. On the
262 other hand, although PDMS is a membrane material widely used, so far the manufacture
263 of industrial-scale PDMS membrane modules is scarce. Thus, a unitary price of €30 per
264 m^2 of membrane was assumed in this study, which represent a competitive price among
265 industrial membrane technology.

266 Due to uncertainty on considered conversion factors, the influence of input factors on
267 energy, environmental and economic assessment was evaluated by means of a sensitive
268 and uncertainty analysis based on Monte Carlo calculations. The Standardized Regression
269 Coefficients (SRCs) method was selected as sensitivity analysis technique. SRC was
270 performed using Monte Carlo calculations applying semi-random Latin Hypercube
271 Sampling (LHS) method [42]. A value of 0.7 was established as the minimum coefficient
272 of determination (R^2) required for validating the standardized regression slope (β_i) as
273 sensitivity measure [43]. Moreover, when applying linear models as the ones used in this

study, R^2 is close to 1 and SRC can be used to screen influential and non-influential factors. Inputs resulting in β_i higher than 0.1 were selected as influential factors. The number of Monte Carlo calculations was set to 10000. Uncertainty was assessed by the mean and 10th and 90th percentiles of Monte Carlo outputs [44]. Table 3 summarizes the ranging of each input factor considered. The evaluated outputs were the energy balance (EB), the GHG emissions (GHG) and the payback period (PB).

Table 3. Ranging of considered inputs in Monte Carlo calculations.

Conversion factors	Nomenclature	Default (min-max)
CH_4 power energy conversion efficiency (%)	ECE	35 (30 - 40)
Energy cost (€ per kWh)	EC	0.07 (0.05 - 0.09)
Membrane cost (€ per m^2)	MC	30 (25 - 35)*
GHG from Spain energy mix ($kgCO_2$ per kWh)	EM	0.35** (0.3 - 0.4)

*Calculated from a membrane nominal price increase/decrease of the 15%.
**Calculated from the IPCC 2013 GWP 100a V1.03 methodology.

3. RESULTS AND DISCUSSION

3.1. Performance of the degassing membrane system

Fig. 2 shows the methane flux and the methane recovery efficiency achieved within the different operating conditions evaluated. As this figure shows, the methane flux through the membrane grew by increasing the Q_L until reaching a "critical" Q_L value from which methane flux declined as Q_L was raised. Besides, both the methane flux and the "critical" Q_L were influenced by the applied TMP, reaching higher methane fluxes and higher "critical" Q_L values as TMP raises. In this respect, raising the liquid velocity though the shell of the DM favored turbulent flow, so improving the mass transference in the liquid phase. Consequently, the methane flux through the membrane was enhanced, achieving higher recovered methane flows. Nevertheless, the increase in the liquid flow rate reduced

294 the hydraulic retention time in the DM, decreasing the time contact between liquid and
295 membrane thus reducing MRE (see Fig. 2b). Moreover, the obtained results show a lineal
296 dependency between MRE and Q_L at each TMP level evaluated. Indeed, maximum MRE
297 would be reached at 'batch' conditions, as predicted by the linear fit of the results
298 obtained. Although according to *eq*. 10, MRE should present an exponential dependency
299 on Q_L, the exponential term can be resembled to a linear expression for relatively high
300 liquid fluxes. The obtained results are in agreement with the results reported by Cookney
301 *et al*. [13], displaying a lineal dependency of MRE on the superficial liquid velocity when
302 values above 0.01 m s^{-1} were applied.

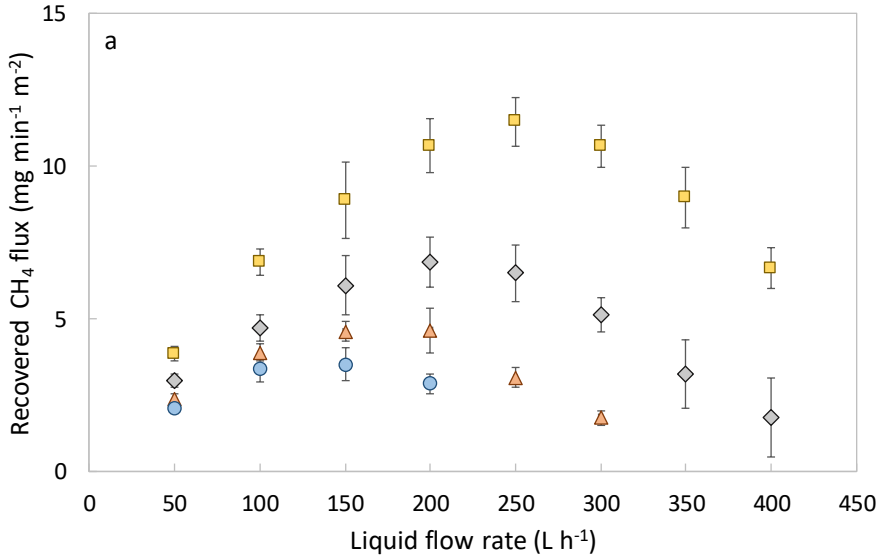

303

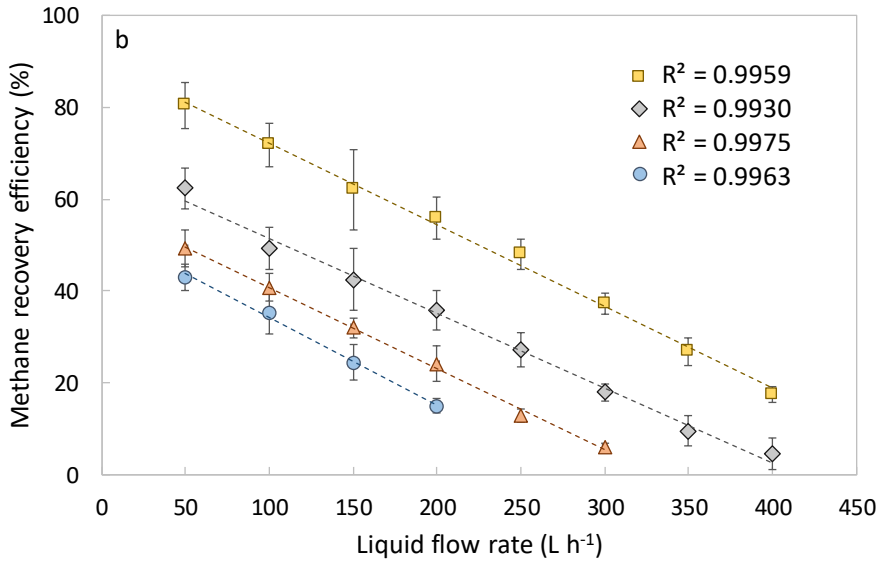

304

Fig. 2. Methane recoveries for the different operating conditions tested: (a) Recovered methane flux and (b) Methane recovery efficiency. Dotted lines represents a linear fit. ◻ TMP of 0.8 bars; ◇ TMP of 0.6 bars; △ TMP of 0.4 bars; ○ TMP of 0.2 bars.

On the other hand, as Fig. 2 shows, methane recovery raised as the TMP was increased. As reported by different authors [45-47], the effect of TMP on membrane permeability depends on both the nature of the gas treated and the material and thickness of the membrane contactor used. In this regard, a favorable effect of vacuum pressure on methane recoveries [26] and methane mass transfer coefficients [28] has been observed when using PDMS membranes. Therefore, increasing TMP could result in an increase in the membrane permeability for methane, achieving better recoveries. Indeed, this kind of behavior has been reported with similar organic compounds (such as C_3H_8 or C_4H_{10}) when using dense silicone rubber membranes [48]. Moreover, raising TMP can also produce an improvement in the driving force by the reduction of the methane partial pressure at the gas phase, thus improving mass flux. As suggested by other authors (*e.g.* Henares *et al.*, [27]), the methane concentration reached in the membrane-gas interphase (c^*) could not be negligible compared to the methane concentration dissolved in the water ($[CH_4]_{dis}$), directly affecting the calculated K_O. Nonetheless, further research would be needed to confirm this hypothesis.

3.2. Effect of operating conditions on overall mass transfer coefficient

Since recovered methane flux mainly depends on the overall mass resistance, the effect of Q_L and TMP on K_O was evaluated in order to determine the operational conditions under which methane capture is maximized. To this aim, K_O was modelled using *eq*. 9. As Fig. 3 illustrates, Q_L and TMP strongly affected K_O, denoting that both liquid and membrane resistances play a key role on establishing the overall resistance to the mass flux. According to *eq*. 9, if liquid resistance is not negligible, k_L should raise as Q_L is

330 increased, consequently increasing K_O. Nevertheless, the obtained results reveal that K_O
331 increased until a maximum value, from which K_O decreased as Q_L was increased. This
332 phenomenon could be explained by two possible hypotheses. (1) On the one hand, the
333 decrease observed on K_O could be explained by the hydrodynamics of the system.
334 According to Henares *et al.* [28], membrane units could present a liquid flow rate limit
335 from which the membrane fibers may suffer some kind of shakings, deforming and
336 compressing, thereby reducing their effectivity. Besides, the operation at elevated liquid
337 velocities of high fiber-density membrane contactors could favor the formation of dead
338 zones [26], being this effect intensified when working by shell side. Thus, K_O could suffer
339 a reduction since a fraction of the total membrane area is inefficiently used. (2) On the
340 other hand, the decrease observed in K_O could also be the results of the formation of an
341 additional resistance to mass flux. Since the DM was fed with effluent from an AnMBR
342 (solids free stream), a fouling resistance could have appeared due to colloids deposition
343 or salts precipitation onto the membrane surface [49], or soluble organic products
344 adsorption on the membrane [50]. Additionally, in pressure-driven membrane systems
345 other undesirable effects can appear, such as concentration polarization due to high
346 concentration gradients opposite to flux. Hence, further research would be needed to
347 confirm these hypotheses and determine which one(s) of the above-mentioned effects
348 affected the overall resistance to mass flux.

349 Regarding the influence of TMP on K_O, Fig. 3 shows that increasing the vacuum pressure
350 can enhance the overall mass transfer coefficient. As previously commented, an
351 improvement of membrane permeability is expected when rising the TMP, reducing
352 membrane resistance and enhancing mass flux. Finally, since increasing K_O means
353 improving methane flux, operating conditions must be optimized in order to enhance the
354 economic feasibility of PDMS DMs for dissolved methane capture. Fig. 4 shows the

operating conditions under which K_O was maximum. The results shown in this figure allow establishing the optimum Q_L-TMP relation under which permeated methane flux is maximized.

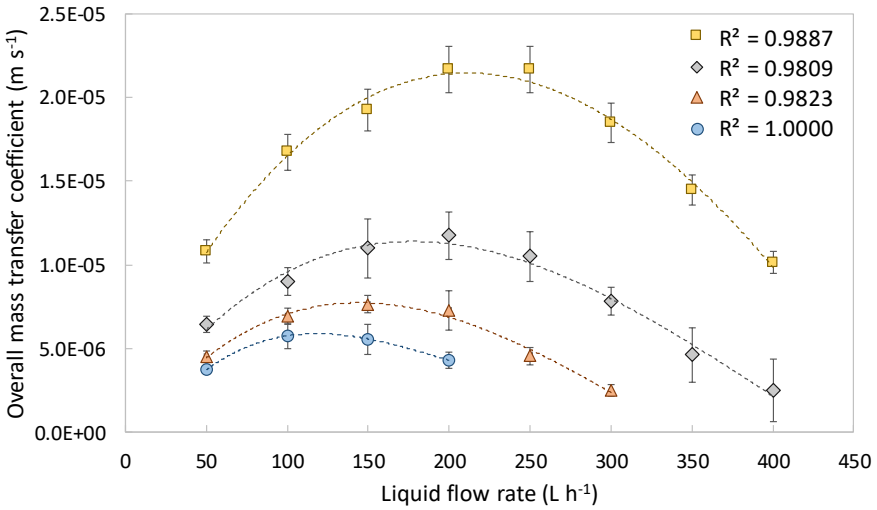

Fig. 3. Effect of transmembrane pressure (TMP) and liquid flow rate on the overall mass transfer coefficient (K_O). Dotted lines represent a third-order polynomial fit. ◻ TMP of 0.8 bars; ◇ TMP of 0.6 bars; △ TMP of 0.4 bars; ○ TMP of 0.2 bars.

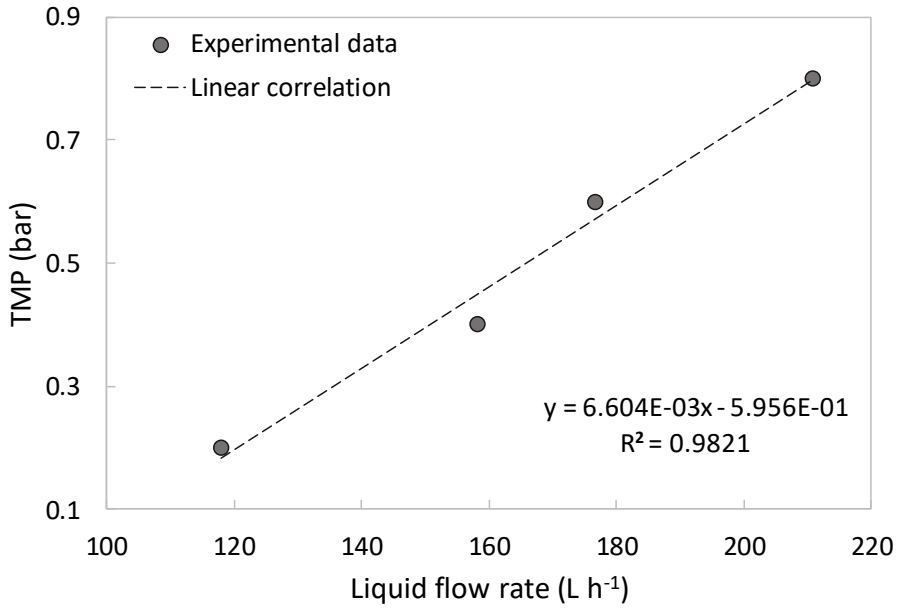

Fig. 4. Operating Q_L-TMP relation under which K_O is maximized for the evaluated DM. Dotted line represents a linear fit.

3.3. Quality and quantity of the recovered gas

Fig. 5 shows the recovered permeate gas flow rate (Q_G) and the methane fraction in the recovered gas for the different operational condition tested. As can be seen in Fig. 5, the increase in TMP raises Q_G. As above explained, this effect seems due to an enhancement in membrane permeability as well as a reduction in the partial pressure of the gas phase, enabling higher gas fluxes. Moreover, Q_G increased with Q_L until reaching a maximum for which Q_G remained constant. In this case, the growth of Q_G was related to the reduction in the resistance to the methane flux (reflected by the growth in the overall mass transfer coefficient) consequence of the increase in Q_L. Thus, when K_O reached the maximum value, Q_G was not significantly affected by Q_L.

Similarly, the methane content in the permeate gas was also strongly affected by the operational TMP and Q_L, achieving higher methane fractions in the gas when the K_O reached a maximum value. Furthermore, the maximum methane content in the recovered gas was achieved at the lowest TMP tested, decreasing as TMP was raised (see Fig. 5). This effect is due to the higher PDMS permeability of other gases dissolved in the anaerobic effluent, such as CO_2, H_2S and NH_3 [45,51], increasing therefore the recovery of these gases when the driving force is increased. However, as different author showed [52,53], methane permeability/selectivity on PDMS is affected by the presence/concentration of other gases in the treated stream. Thus, both Q_G and gas composition may be strongly influenced by the treated effluent composition.

Otherwise, it is important to consider that the methane content in the mixture of produced biogas and recovered dissolved methane should be higher than 35%, which represents the minimum threshold limit for valorization in commercial microturbines [54]. Table 4 shows the methane fraction in the gas recovered from dissolved methane capture by

different technologies. As this table shows, stripping methane processes and biological systems generally results in low methane contents in captured gases due to high air injection requirements thereby not permitting direct energy conversion from recovered dissolved methane. On the other hand, permeable PDMS DMs seem to be able to achieve methane fractions in captured gas similar to the ones reported when using porous membranes despite of their higher permeability of other gases. Indeed, in this study, the methane content in the gas recovered from dissolved methane capture was up to 42, 29, 30 and 31% for a TMP of 0.2, 0.4, 0.6 and 0.8 bar, respectively. Thus, the mixing of this recovered gas and the biogas produced in the AnMBR could be directly valorized.

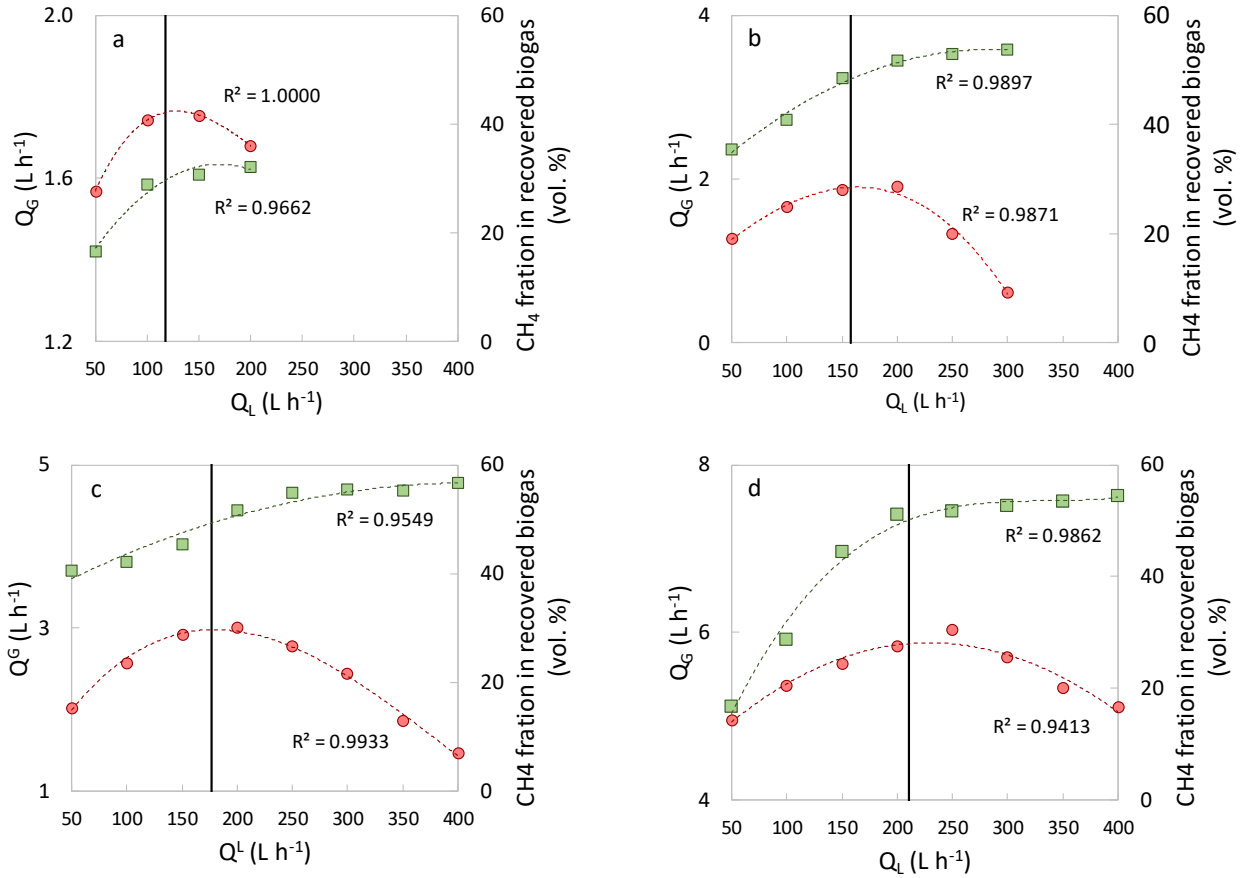

Fig. 5. Recovered permeate gas flow rate (Q_G) and methane fraction in recovered gas as a function of Q_L for a TMP of: (a) 0.2, (b) 0.4, (c) 0.6 and (d) 0.8 bars. Dotted lines represent a third-order polynomial fit. Solid lines represent the maximum K_O obtained from Fig. 3. Q_G. Methane fraction in recovered gas.

Table 4. Methane fractions achieved in the recovered gas by different dissolved methane capture technologies.

Treatment system	Methane fraction in captured gas (%)	Reference
Diffused aeration	4 - 0.5	[55]
Free-fall jet tower	6 - 0.5	[55]
Down-flow hanging sponge reactor (DHSR)	None	[19]
Two-in-series DHSR	37	[20]
Porous (multi-layered composite) DM operated at vacuum filtration	22 - 20	[29]
Porous (multi-layered composite) DM operated at vacuum filtration	52	[30]
Permeable (PDMS) DM operated at high sweep gas flow rates	0.028*	[56]
Porous (PP) and permeable (PDMS) DMs operated at low liquid velocities and sweep gas	53*	[13]

*Calculated from a mass balance by the authors.

3.4. Energy, environmental and economic feasibility of the system

PDMS DM feasibility was assessed for three different targets: energy demand, environmental impact and economics of the system. Fig. 6 shows the obtained results from the analysis, were default values results are represented by columns. Error intervals represent the 10^{th} and 90^{th} percentiles of Monte Carlo results. Fig. 6a shows the recovered energy per volume of effluent treated versus Q_L for each TMP tested. It must be highlight the positive energy balance achieved under all the operating conditions tested in this study. Indeed, a net energy production from methane can be achieved by using PDMS DM technology for capturing the methane dissolved in the effluent from AnMBR. The maximum energy recovery was reached at the highest TMP and the lowest Q_L applied. From these results it can be concluded that, although operating at elevated TMP involve

higher energy demands, these can be overcome by the energy recovered from the captured methane, enhancing the energy balance of AnMBR technology. On the other hand, operating at reduced Q_L seems also to improve energy recovery by increasing MRE (see Fig. 2b). Similarly, as Fig. 6b shows, the lowest GHG emission was reached at the highest TMP and the lowest Q_L due to the improvement in the methane capture and energy recovery under these conditions. Therefore, it could be assumed that low Q_L might be applied in order to improve the energy and environmental feasibility of PDMS DM technology.

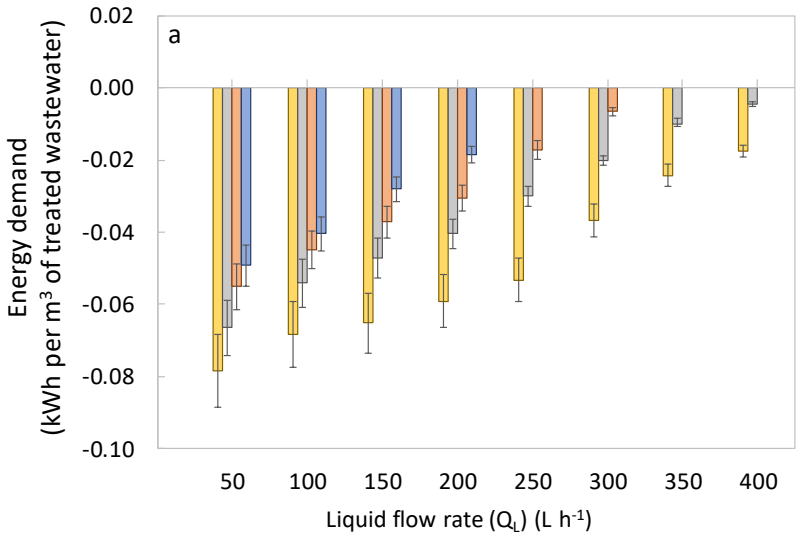

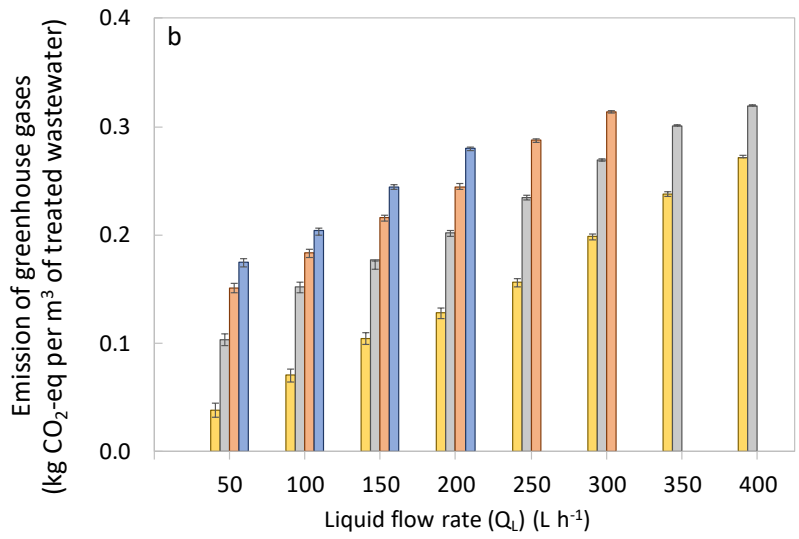

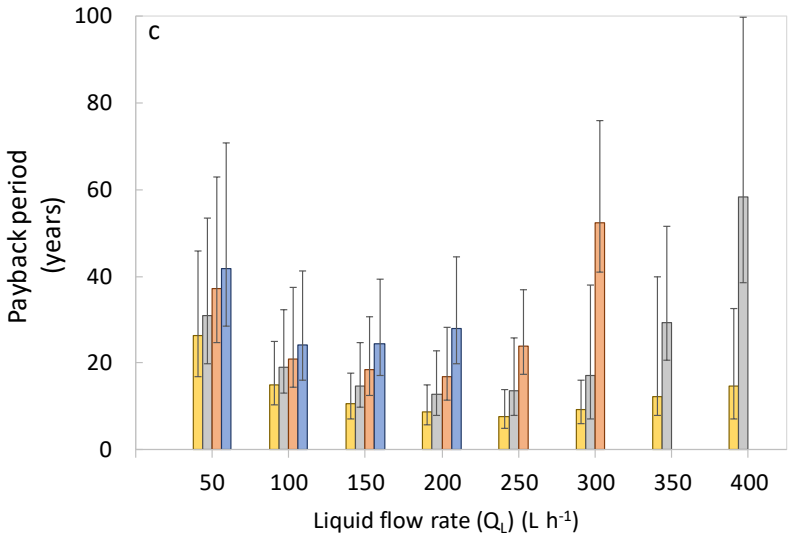

Fig. 6. Feasibility of PDMS DMs for methane capture from AnMBR effluents: (a) net energy demand, (b) GHG emissions, and (c) payback period. Missing columns are due to lack of experimental results. Error bars represent uncertainties at 10 and 90% of confidence calculated from Monte Carlo simulations. ■ TMP of 0.8 bars; ■ TMP of 0.6 bars; ■ TMP of 0.4 bars; ■ TMP of 0.2 bars.

However, operating a DM at low Q_L could be a non-viable solution since it would mean high membrane area requirements. Therefore, since increasing membrane area requirements results in increasing capital expenses (CAPEX), a compromise in the operational Q_L:A ratio must be reached. Hence, a payback study was carried out to determine the most favorable operational conditions focusing on an economic target. Fig. 6c displays the results from the payback estimation conducted in this study. As this figure shows, DM technology is able to reach competitive payback periods, highlighting the potential scaling-up feasibility of this technology for methane capture from AnMBR effluents. Operating at low Q_L entails non-feasible performances due to the significant increase in CAPEX, while operating at high Q_L involves high operating expenses (OPEX) due to low MREs. An economic optimum can be observed in this study when operating at TMP values around 0.8 bars and Q_L levels of about 250 L h^{-1}. These values resulted in a Q_L:A ratio around 100 L m^{-2} h^{-1} achieving a payback period of around 7.5 years.

Table 5 shows the results obtained from the SRC analysis. As this table illustrates, high correlations (nearby 1) were obtained due to the linearity of the model used, allowing the

446 detection of the most influent inputs on each balance. As expected, the sole influent input
447 factor on energy balance was the energy conversion efficiency since the other inputs are
448 not related to energy generation. Similarly, GHG was influenced by the GHG emissions
449 from the energy mix and the energy conversion efficiency. Indeed, the impact of these
450 two inputs on GHG output was similar in all performed assays (β value around 0.7).
451 Finally, the payback period output was significantly influenced by the different
452 considered inputs (i.e. the energy conversion efficiency, and the energy and membrane
453 costs), being the energy cost the most influential factor. Consequently, uncertainties from
454 energy and GHG emission calculations could be considered assumable, while
455 uncertainties on payback estimations are significantly higher due to the strong influence
456 of the different factors considered.

457

Table 5. Determination of influential inputs according to SRC analysis.

			TMP (bar)											
			0.2			0.4			0.6			0.8		
			β_i											
			EB[a]	GHG[b]	PB[c]	EB[a]	GHG[b]	PB[c]	EB[a]	GHG[b]	PB[c]	EB[a]	GHG[b]	PB[c]
Q_L ($L\ h^{-1}$)	50	R^2	1.000	0.997	0.973	1.000	0.997	0.973	1.000	0.996	0.972	1.000	0.996	0.971
		ECE[d]	-1.000	-0.704	-0.391	-1.000	-0.714	-0.395	-1.000	-0.730	-0.411	-1.000	-0.760	-0.443
		EC[e]	0.000	0.000	-0.786	0.000	0.000	-0.780	0.000	0.000	-0.773	0.000	0.000	-0.758
		MC[f]	0.000	0.000	0.448	0.000	0.000	0.444	0.000	0.001	0.441	0.000	0.001	0.432
		EM[g]	0.000	-0.698	0.001	0.000	-0.690	0.001	0.000	-0.673	0.000	0.000	-0.639	0.000
	100	R^2	1.000	0.997	0.973	1.000	0.997	0.973	1.000	0.997	0.972	1.000	0.996	0.972
		ECE[d]	-1.000	-0.702	-0.390	-1.000	-0.711	-0.392	-1.000	-0.719	-0.400	-1.000	-0.741	-0.422
		EC[e]	0.000	0.000	-0.788	0.000	0.000	-0.781	0.000	0.000	-0.777	0.000	0.000	-0.768
		MC[f]	0.000	0.000	0.449	0.000	0.001	0.445	0.000	0.001	0.443	0.000	0.001	0.438
		EM[g]	0.000	-0.698	0.002	0.000	-0.693	0.000	0.000	-0.684	0.000	0.000	-0.661	0.000
	150	R^2	1.000	0.997	0.973	1.000	0.997	0.973	1.000	0.997	0.972	1.000	0.996	0.972
		ECE[d]	-1.000	-0.704	-0.386	-1.000	-0.710	-0.391	-1.000	-0.717	-0.398	-1.000	-0.734	-0.415
		EC[e]	0.000	0.000	-0.783	0.000	0.000	-0.781	0.000	0.000	-0.778	0.000	0.000	-0.771
		MC[f]	0.000	0.000	0.446	0.000	0.000	0.445	0.000	0.001	0.444	0.000	0.001	0.440
		EM[g]	0.000	-0.700	-0.001	0.000	-0.694	0.000	0.000	-0.687	0.000	0.000	-0.668	0.000
	200	R^2	1.000	0.997	0.973	1.000	0.997	0.973	1.000	0.997	0.972	1.000	0.996	0.972
		ECE[d]	-1.000	-0.705	-0.386	-1.000	-0.710	-0.391	-1.000	-0.718	-0.399	-1.000	-0.732	-0.413
		EC[e]	0.000	0.000	-0.783	0.000	0.000	-0.781	0.000	0.000	-0.778	0.000	0.000	-0.772
		MC[f]	0.000	0.001	0.446	0.000	0.000	0.445	0.000	0.001	0.444	0.000	0.001	0.440
		EM[g]	0.000	-0.700	0.000	0.000	-0.694	0.000	0.000	-0.686	0.000	0.000	-0.671	0.000
	250	R^2				1.000	0.997	0.973	1.000	0.997	0.972	1.000	0.996	0.972
		ECE[d]				-1.000	-0.712	-0.393	-1.000	-0.722	-0.402	-1.000	-0.733	-0.414
		EC[e]				0.000	0.000	-0.780	0.000	0.000	-0.776	0.000	0.000	-0.772
		MC[f]				0.000	0.000	0.445	0.000	0.001	0.443	0.000	0.001	0.440
		EM[g]				0.000	-0.693	0.000	0.000	-0.682	0.000	0.000	-0.670	0.000

	300	R^2		1.000	0.997	0.972	1.000	0.996	0.972	1.000	0.996	0.972
		ECE[d]		-1.000	-0.719	-0.400	-1.000	-0.735	-0.416	-1.000	-0.737	-0.418
		EC[e]		0.000	0.000	-0.777	0.000	0.000	-0.771	0.000	0.000	-0.770
		MC[f]		0.000	0.001	0.443	0.000	0.001	0.439	0.000	0.001	0.440
		EM[g]		0.000	-0.685	0.000	0.000	-0.668	0.000	0.000	-0.666	0.000
	350	R^2					1.000	0.996	0.929	1.000	0.996	0.972
		ECE[d]					-1.000	-0.735	-0.775	-1.000	-0.747	-0.428
		EC[e]					0.000	0.000	-0.484	0.000	0.000	-0.765
		MC[f]					0.000	0.001	0.277	0.000	0.001	0.436
		EM[g]					0.000	-0.667	0.003	0.000	-0.655	0.000
	400	R^2					1.000	0.996	0.971	1.000	0.996	0.971
		ECE[d]					-1.000	-0.762	-0.445	-1.000	-0.779	-0.465
		EC[e]					0.000	0.000	-0.757	0.000	0.000	-0.748
		MC[f]					0.000	0.001	0.432	0.000	0.001	0.426
		EM[g]					0.000	-0.637	0.000	0.000	-0.616	0.000

[a]EB: Energy Balance.
[b]GHG: GreenHouse gases emission.
[c]PB: PayBack.
[d]ECE: Energy Conversion Efficiency.
[e]EC: Energy Cost.
[f]MC: Membrane Cost.
[g]EM: GHG from Energy Mix.

The feasibility of coupling a PDMS DM together with an AnMBR (AnMBR+DM) for UWW treatment was also evaluated. Three different scenarios were considered to carry out this assessment: i) AnMBR+DM_a, where DM is operated at economical optimum (0.8 bar and 250 L h^{-1} of TMP and Q_L, respectively); ii) AnMBR+DM_b, where DM is operated at energy recovery and GHG mitigation maximum capacity (0.8 bar and 50 L h^{-1} of TMP and Q_L, respectively); and iii) AnMBR+DM_c, where DM is operated under a compromise between methane recovery and economic viability (0.8 bar and 150 L h^{-1} of TMP and Q_L, respectively). The obtained results were compared to typical values from other technologies for UWW treatment. As Table 6 shows, the AnMBR+DM combination would enable to reduce significantly the energy cost and carbon footprint of UWW treatment, achieving even net energy productions. In addition, feasible payback periods can be achieved when energy and environmental aspects are also considered in the DM operation (e.g. AnMBR+DM_c scenario). Thus, AnMBR+DM can be regarded as an interesting alternative for low-strength wastewaters treatment. In fact, considering the AnMBR+DM_c alternative as the more suitable scenario (i.e. combining energy, environmental and economic targets), energy demands and GHG emissions of -0.04 kWh and 0.113 kg of CO_2-eq per m^3 of treated water can be archived, respectively, resulting in payback periods of about 10.5 years.

Table 6. Comparison of different technologies for UWW treatment.

Treatment system	Energy demands (kWh m^{-3})	GHG emissions (kg CO_2-eq m^{-3})	DM payback period (years)	Reference
AnMBR + DM_a	- 0.027	0.165	26.0	This study
AnMBR + DM_b	- 0.051	0.048	7.5	This study
AnMBR + DM_c	- 0.038	0.114	10.5	This study
AnMBR at 18 ºC	0.025	0.308	-	[33]
Conventional activated sludge	0.30 - 0.60	0.093 - 0.186*	-	[1,57]

Extended aeration	0.34 - 0.82	0.105 - 0.254*	-	[58]
Aerobic MBR	0.50 - 1.00	0.155 - 0.310*	-	[59,60]

*Calculated from reported energy demands
AnMBR+DMa: DM operated at economical optimum
AnMBR+DMb: DM operated for maximum GHG mitigation and energy recovery
AnMBR+DMc: DM operated under a compromise between methane recovery and economic viability

4. CONCLUSIONS

PDMS DM technology was used for capturing the methane dissolved in the effluent from an AnMBR prototype-plant. The main findings from the PDMS DM performance were:

- Methane recovery was maximized at high TMP and low Q_L. Maximum methane recovery efficiencies of around 80% were achieved when operating at 0.8 bars and 50 L h^{-1}.

- An improvement on the K_O was observed by increasing TMP. High operating Q_L can produce an unfavorable effect on methane recovery by a reduction on K_O.

- Both Q_G and methane fraction in recovered gas are strongly influenced by the operating Q_L and TMP. A maximum methane fraction of about 40% was achieved when operating at 0.2 bar and around 110 L h^{-1}, coinciding with the maximum K_O reached at this TMP.

Moreover, the feasibility of the combination AnMBR+DM for UWW treatment was evaluated. The main findings from this combination were:

- A TMP of 0.8 bar and Q_L of 150 L h^{-1} resulted in optimum performance in terms of energy recovery, GHG emissions and economic feasibility.

- DM allowed enhancing the energy recovery while reducing the GHG emissions of the AnMBR prototype-plant. Indeed, the AnMBR+DM resulted in energy

demands and GHG emissions of -0.04 kWh and 0.113 kg of CO_2-eq per m^3 of treated water, respectively.

- The economic evaluation proven the feasibility of DM for scaling-up AnMBR technology for UWW treatment. A payback period of around 10.5 years was estimated for the evaluated DM when a compromise between methane recovery and economic viability was established. A payback period of about 7.5 years can be achieved when operating the DM at economic optimum.

ACKNOWLEDGEMENTS

This research work was supported by Generalitat Valenciana via the fellowships CPI-16-155 and C12747, as well as the financial aid received from Ministerio de Economía y Competitividad via Juan de la Cierva contract FJCI-2014-21616. This research work was also possible thanks to co-finance of the European financial instrument for the Environment (LIFE+) during the implementation of the Project Membrane for ENERGY and WATER RECOVERY "MEMORY" (LIFE13 ENV/ES/001353).

REFERENCES

[1] McCarty, P. L., Bae, J., & Kim, J. (2011). Domestic wastewater treatment as a net energy producer - can this be achieved? *Environmental Science & Technology*, 45(17), 7100–7106.

[2] Pretel, R., Shoener, B. D., Ferrer, J., & Guest, J. S. (2015). Navigating environmental, economic, and technological trade-offs in the design and operation of submerged

528 anaerobic membrane bioreactors (AnMBRs). *Water Research*, 87, 531–541.

529 [3] Guest, J.S., Skerlos, S.J., Barnard, J.L., Beck, M.B., Daigger, G.T., Hilger, H.,
530 Jackson, S.J., Karvazy, K., Kelly, L., Macpherson, L., Mihelcic, J.R., Promanik, A.,
531 Raskin, L., van Loosdrecht, M.C.M., Yeh, D., Love, N.G., (2009). A new planning
532 and design paradigm to achieve sustainable resource recovery from wastewater.
533 *Environ. Sci. Technol.* 43, 6126–6130.

534 [4] Smith, A. L., Stadler, L. B., Love, N. G., Skerlos, S. J., & Raskin, L. (2012).
535 Perspectives on anaerobic membrane bioreactor treatment of domestic wastewater:
536 A critical review. *Bioresource Technology*, 122, 149–159.

537 [5] Robles, Á., Ruano, M. V., Charfi, A., Lesage, G., Heran, M., Harmand, J., Seco, A.,
538 Steyer, J-P., Batstone, D.J., Kim, J. & Ferrer, J. (2018). A review on anaerobic
539 membrane bioreactors (AnMBRs) focused on modelling and control aspects.
540 *Bioresource Technology*, 270, 612–626.

541 [6] Wang, W., Yang, Q., Zheng, S., Wu, D. (2013). Anaerobic membrane bioreactor
542 (AnMBR) for bamboo industry wastewater treatment. *Bioresour. Technol.* 149,
543 292–300.

544 [7] Pretel, R., Robles, A., Ruano, M. V., Seco, A., & Ferrer, J. (2014). The operating
545 cost of an anaerobic membrane bioreactor (AnMBR) treating sulphate-rich urban
546 wastewater. *Separation and Purification Technology*, 126, 30–38.

547 [8] Xia, T., Gao, X., Wang, C., Xu, X., Zhu, L. (2016). An enhanced anaerobic
548 membrane bioreactor treating bamboo industry wastewater by bamboo charcoal
549 addition performance and microbial community analysis. *Bioresour. Technol.* 220,
550 26–33.

551 [9] Aslam, M., McCarty, P.L., Shin, C., Bae, J., Kim, J. (2017a). Low energy single-
552 staged anaerobic fluidized bed ceramic membrane bioreactor (AFCMBR) for
553 wastewater treatment. *Bioresour. Technol.* 240, 33–41.

554 [10] Aslam, M., Charfi, A., Lesage, G., Heran, M., Kim, J. (2017b). Membrane
555 bioreactors for wastewater treatment: a review of mechanical cleaning by scouring
556 agents to control membrane fouling. *Chem. Eng. J.* 307, 897–913.

557 [11] Giménez, J. B., Martí, N., Ferrer, J., & Seco, A. (2012). Methane recovery efficiency
558 in a submerged anaerobic membrane bioreactor (SAnMBR) treating sulphate-rich
559 urban wastewater: Evaluation of methane losses with the effluent. *Bioresource*
560 *Technology*, 118, 67–72.

561 [12] Giménez, J. B., Martí, N., Robles, A., Ferrer, J., & Seco, A. (2014). Anaerobic
562 treatment of urban wastewater in membrane bioreactors: Evaluation of seasonal
563 temperature variations. *Water Science and Technology*, 69(7), 1581–1588.

564 [13] Cookney, J., Mcleod, A., Mathioudakis, V., Ncube, P., Soares, A., Jefferson, B., &
565 McAdam, E. J. (2016). Dissolved methane recovery from anaerobic effluents using
566 hollow fibre membrane contactors. *Journal of Membrane Science*, 502, 141–150.

567 [14] Heile, S., Chernicharo, C. A. L., Brandt, E. M. F., & McAdam, E. J. (2017).
568 Dissolved gas separation for engineered anaerobic wastewater systems. *Separation*
569 *and Purification Technology*, 189, 405–418.

570 [15] Stanojević, M., Lazarević, B., Radić, D. (2003). Review of membrane contactors
571 designs and applications of different modules in industry. *FME Trans.* 31, 91–98.

572 [16] Chen, S. and Smith, A.L. (2018). Methane-driven microbial fuel cells recover energy

573 and mitigate dissolved methane emissions from anaerobic effluents, Environ. Sci.
574 Water Res. Technol. 4, 67–79.

575 [17] Raghoebarsing, A. A. et al. (2006). A microbial consortium couples anaerobic
576 methane oxidation to denitrification, Nature, 440(7086), 918–921.

577 [18] Knittel K. and Boetius A. (2009). Anaerobic oxidation of methane: progress with an
578 unknown process, Annu. Rev. Microbiol. 63, 311–334.

579 [19] Hatamoto M., Yamamoto H., Kindaichi T., Ozaki N., Ohashi A. (2010). Biological
580 oxidation of dissolved methane in effluents from anaerobic reactors using a down-
581 flow hanging sponge reactor. *Water Res.* 44, 1409–1418.

582 [20] Matsuura, N. et al. (2010). Closed DHS system to prevent dissolved methane
583 emissions as greenhouse gas in anaerobic wastewater treatment by its recovery and
584 biological oxidation, Water Sci. Technol., 61(9), 2407–2415.

585 [21] Myung, J., Saikaly, P.E., Logan, B.E. (2018). A two-staged system to generate
586 electricity in microbial fuel cells using methane. Chem. Eng. J. 352, 262e267.

587 [22] Yu, L., Yang, Z., He, Q., Zeng, R.J., Bai, Y., Zhou, S. (2018). Novel gas diffusion
588 cloth bioanodes for high-performance methane-powered microbial fuel cells.
589 Environ. Sci. Technol. 53 (1), 530e538.

590 [23] Chen, S. and Smith A.L. (2019). Performance and microbial ecology of methane-
591 driven microbial fuel cells at temperatures ranging from 25 to 5 °C, Water Res. 166.

592 [24] Crone, B. C., Garland, J. L., Sorial, G. A., & Vane, L. M. (2017). Corrigendum to
593 “Significance of dissolved methane in effluents of anaerobically treated low strength
594 wastewater and potential for recovery as an energy product: A review” *Water*

595 *Research*, 111, 420.

596 [25] Shao, J., et al. (2008). Boiler feed water deoxygenation using hollow fiber membrane
597 contactor. Desalination 234 (1), 370e377.

598 [26] Cookney, J. (2011). Methane management in sewage treatment. *Ph.D. thesis. School*
599 *of applied sciences. Cranfield university, United kingdom.*

600 [27] Henares, M., Izquierdo, M., Penya-Roja, J. M., & Martínez-Soria, V. (2016).
601 Comparative study of degassing membrane modules for the removal of methane
602 from Expanded Granular Sludge Bed anaerobic reactor effluent. *Separation and*
603 *Purification Technology*, 170, 22–29.

604 [28] Henares, M., Izquierdo, M., Marzal, P., & Martínez-Soria, V. (2017).
605 Demethanization of aqueous anaerobic effluents using a polydimethylsiloxane
606 membrane module: Mass transfer, fouling and energy analysis. *Separation and*
607 *Purification Technology*, 186, 10–19.

608 [29] Bandara, W.M.K.R.T.W., Satoh, H., Sasakawa, M., Nakahara, Y., Takahashi, M.,
609 Okabe, S. (2011). Removal of residual dissolved methane gas in an upflow anaerobic
610 sludge blanket reactor treating low-strength wastewater at low temperature with
611 degassing membrane, Water Res. 45, 3533–3540.

612 [30] Bandara, W.M.K.R.T.W., Kindaichi, T., Satoh, H., Sasakawa, M., Nakahara, Y.,
613 Takahashi, M., Okabe, S. (2012). Anaerobic treatment of municipal wastewater at
614 ambient temperature: Analysis of archaeal community structure and recovery of
615 dissolved methane, Water Res. 46 (2012) 5756–5764.

616 [31] Ahmed, T., Semmens, M.J. (1992). Use of sealed end hollow fibers for bubbleless

membrane aeration: experimental studies. J. Membr. Sci. 69 (1e2), 1e10.

[32] Malek, A., Li, K., Teo, W.K. (1997). Modeling of Microporous Hollow Fiber Membrane Modules Operated under Partially Wetted Conditions, Ind. Eng. Chem. Res. 36, 784–793.

[33] Jiménez, A., Ferrer, J., Rogalla, F., Vázquez, J.R., Seco, A., Robles, Á. (2020). Energy and environmental impact of an AnMBR demonstration plant treating urban wastewater. In: Current Developments in Biotechnology and Bioengineering, 1st Edition, Advanced Membrane Separation Processes for Sustainable Water and Wastewater Management - Case Studies and Sustainability Analysis. Editors: Giorgio Mannina Ashok Pandey Christian Larroche How Yong Ng Huu Hao Ngo. Elsevier

[34] Tchobanoglous, G., Burton, B.L., Stensel, H.D. (2003). Wastewater Engineering: Treatment and Reuse. *Metcalf & Eddy, Inc. and The McGraw-Hill Companies Inc., New York*.

[35] Lu, J. G., Zheng, Y. F., Cheng, M. D. (2008). Wetting mechanism in mass transfer process of hydrophobic membrane gas absorption. *Journal of Membrane Science* 308, 180-190.

[36] Wickramasinghe, S. R., Semmens, M. J., & Cussler, E. L. (1993). Hollow fiber modules made with hollow fiber fabric. *Journal of Membrane Science*, 84, 1–14.

[37] EPA. (2017). Catalog of CHP Technologies. Darrow, K., Tidball, R., Wang, J., & Hampson, A. U.S. Environmental Protection Agency Combined Heat and Power Partnership.

639 [38] IPCC. (2014). Climate Change 2014: Synthesis Report. Contribution of Working
640 Groups I, II and III to the Fifth Assessment Report of the Intergovernmental Panel
641 on Climate Change, eds R. K. Pachauri,M. R. Allen, V. R. Barros, J. Broome,W.
642 Cramer, R. Christ, J. A. Church, L. Clarke, Q. Dahe and P. Dasgupta: IPCC.

643 [39] MITECO, 2017. Official website of the Ministry for the ecological transition.
644 Spanish government, Madrid. Retrieved October 5, 2019, from
645 https://www.miteco.gob.es/es/cambio-climatico/temas/mitigacion-politicas-y-
646 medidas/factores_emision_tcm30-479095.pdf.

647 [40] Gesternova energía. (2019). Spanish electricity rates (Tarifa eléctrica España).
648 Retrieved October 5, 2019, from https://gesternova.com/tarifas-luz/tarifas-luz-alta-
649 tension/

650 [41] Aura energía. (2019). Spanish electricity rates (Tarifa eléctrica España). Retrieved
651 October 5, 2019, from https://www.aura-energia.com/tarifas-luz-industria-
652 peninsula/

653 [42] Helton J.C., Davis F.J. (2003) Latin hypercube sampling and the propagation of
654 uncertainty in analyses of complex systems. Reliability Enginnering and System
655 Safety. 81, 23-69

656 [43] Saltelli, A., Tarantola, S., Campolongo, F., Ratto, M. (2004). Sensitivity Analysis in
657 Practice: A Guide to Assessing Scientific Models. John Wiley and Sons.

658 [44] Sin, G., Gernaey, K. V., Neumann, M.B., van Loosdrecht, M.C.M., Gujer, W.
659 (2009). Uncertainty analysis in WWTP model applications: A critical discussion
660 using an example from design, Water Res. 43 2894–2906.

[45] Merkel, T. C., Bondar, V. I., Nagai, K., Freeman, B. D., & Pinnau, I. (2000). Gas sorption, diffusion, and permeation in poly(dimethylsiloxane). *Journal of Polymer Science, Part B: Polymer Physics*, 38(3), 415–434.

[46] Sanders, D. F., Smith, Z. P., Guo, R., Robeson, L. M., McGrath, J. E., Paul, D. R., & Freeman, B. D. (2013). Energy-efficient polymeric gas separation membranes for a sustainable future: A review. *Polymer (United Kingdom)*, 54(18), 4729–4761.

[47] Robeson, L. M., Smith, Z. P., Freeman, B. D., & Paul, D. R. (2014). Contributions of diffusion and solubility selectivity to the upper bound analysis for glassy gas separation membranes. *Journal of Membrane Science*, 453, 71–83.

[48] Favre, E. (2017). Polymeric Membranes for Gas Separation. Elsevier B.V. Nancy Université, France.

[49] Zarebska, A., Amor, Á. C., Ciurkot, K., Karring, H., Thygesen, O., Andersen, T. P., Hägg, M.B., Christensen, K.V., Norddahl, B. (2015). Fouling mitigation in membrane distillation processes during ammonia stripping from pig manure. *Journal of Membrane Science*, 484, 119–132.

[50] Chan, R., & Chen, V. (2004). Characterization of protein fouling on membranes: Opportunities and challenges. *Journal of Membrane Science*, 242(1–2), 169–188.

[51] Robb, W. L. (1968). Thin silicon membranes. Their permeation properties and some applications. *Annals of the New York Academy of Sciences*, 146, 119–137.

[52] Pinnau, I., & He, Z. (2004). Pure- and mixed-gas permeation properties of polydimethylsiloxane for hydrocarbon/methane and hydrocarbon/hydrogen separation. *Journal of Membrane Science*, 244(1–2), 227–233.

683 [53] Raharjo, R. D., Freeman, B. D., Paul, D. R., Sarti, G. C., & Sanders, E. S. (2007).
684 Pure and mixed gas CH4 and n-C4H10 permeability and diffusivity in
685 poly(dimethylsiloxane). *Journal of Membrane Science*, 306(1–2), 75–92.

686 [54] S. Micropower Europe, C.T. Corporation, Microturbines specifications - Brochure,
687 (2018). http://www.micropowereurope.com/APLICACIONES/ (accessed February
688 04, 2020).

689 [55] Glória, R.M., Motta, T.M., Silva, P.V.O., Da Costa, P., Brandt, E.M.F., Souza, C.L.,
690 Chernicharo, C.A.L. (2016). Stripping and dissipation techniques for the removal of
691 dissolved gases from anaerobic effluents, Brazilian J. Chem. Eng. 33, 713–721.

692 [56] Cookney, J., Cartmell, E., Jefferson, B., McAdam, E.J. (2012). Recovery of methane
693 from anaerobic process effluent using poly-di-methyl-siloxane membrane
694 contactors, Water Sci. Technol. 65, 604–610.

695 [57] Shoener, B. D., Bradley, I. M., Cusick, R. D., & Guest, J. S. (2014). Energy positive
696 domestic wastewater treatment: The roles of anaerobic and phototrophic
697 technologies. *Environmental Sciences: Processes and Impacts*, 16(6), 1204–1222.

698 [58] Yang, L., Zeng, S., Chen, J., He, M., & Yang, W. (2010). Operational energy
699 performance assessment system of municipal wastewater treatment plants. *Water*
700 *Science and Technology*, 62(6), 1361–1370.

701 [59] Buer, T., & Cumin, J. (2010). MBR module design and operation. *Desalination*,
702 250(3), 1073–1077.

703 [60] Krzeminski, P., van der Graaf, J. H. J. M., & van Lier, J. B. (2012). Specific energy
704 consumption of membrane bioreactor (MBR) for sewage treatment. *Water Science*

705 *& Technology*, 65(2), 380.